Polarization properties of R Cas SiO masers

K. A. Assaf[1], P. J. Diamond[2], A. M. S. Richards[1] and M. D. Gray[1]

[1]University of Manchester, Oxford Road, Manchester, M13 9PL, UK
email: `kam@jb.man.ac.uk`

[2]CSIRO Astronomy and Space Sciences, PO Box 76, Epping, NSW 1710, Australia
email: `philip.diamond@csiro.au`

Abstract. Silicon monoxide maser emission has been detected in the circumstellar envelopes of many evolved stars. It is a good tracer of the wind dynamics within a few stellar radii of the central star. We investigated the polarization morphology in the circumstellar envelope of an AGB star, R Cas, by using the VLBA to map the linear and circular polarization of the v=1, J=1-0 SiO maser transition during 23 epochs over two stellar cycles. The average fractional circular polarization is a few percent. The average fractional linear polarization per epoch is 11–58%, but some isolated features exceed 100%, probably because the total intensity emission is smoother and more resolved-out. The maser electric polarization vector angle has a preferential tendency to be either parallel or perpendicular to the radial direction to the star.

Keywords. masers – polarization – star: AGB – star: late-type star: individual: R Cas.

1. Introduction

The circumstellar envelope (CSE) of an asymptotic giant branch (AGB) star is a very active region. Mass loss from AGB stars is an important means of enriching the stellar medium with processed material. The nature of material returned to the ISM (molecular, dusty and/or ionised) is affected by the inhomogeneity and asymmetry of the stellar wind, and the magnetic field may have a significant influence over these properties. If maser polarization is magnetic in origin, the polarization morphology and linear polarization position angle provides information about the structure of the magnetic field in the CSE.

43-GHz SiO maser images typically show a ring with a radius of a few stellar radii (within the dust formation zone). The maser emission is significantly linearly polarized but circular polarization is weaker, as expected for a non-paramagnetic molecule. The linear and circular polarization percentages are given by:

$$m_\ell = \frac{P}{I} = \frac{\sqrt{(Q^2 + U^2)}}{I} \tag{1.1}$$

$$m_c = \frac{V}{I} \tag{1.2}$$

Herpin *et al.* (2006) found that Mira variables have average values of $m_\ell \sim 30\%$ and $m_c \sim 0.9\%$, respectively. The typical values of m_c suggest a magnetic field strength of few Gauss, if the standard Zeeman interpetation is adopted (Elitzur 1996, as applied to TX Cam by Kemball & Diamond 1997). This model predicts that a radial, stellar-centred magnetic field would produce tangential polarization vectors from emission originating in the plane of the sky containing the star.

Alternatively, even in the absence of a magnetic field, maser pumping by an anisotropic, stellar radiation field could produce strongly polarized maser emission (Western *et al.* 1983). This mechanism might cause the tangential polarization seen in VLBA SiO maser images (Desmurs *et al.* 2000). High-resolution full polarization VLBA imaging of SiO
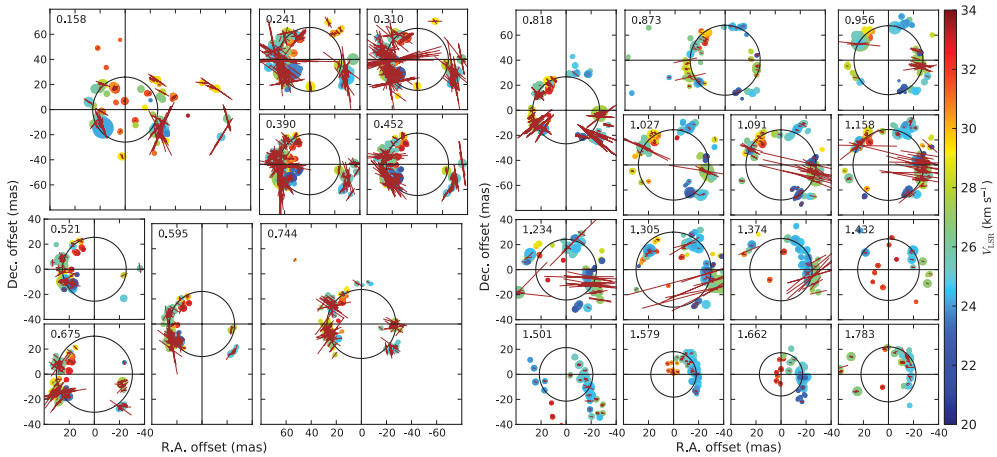
Figure 1. Polarization morphology of R Cas SiO masers. Each pane is labelled with the stellar phase. Symbol size is proportional to total intensity. The vectors show the orientation of the EVPA, length proportional to P.

masers resolves the winds of nearby stars on scales less than 0.1 AU, at high spectral resolution, testing the predictions of these models. We monitored the Mira R Cas, at $\sim$ 176 AU (Vlemmings *et al.* 2003), over 2 stellar cycles, in the 43-GHz SiO $v = 1$ $J = 1 - 0$ line. The data analysis, variability and morphology of the total intensity emission were published by Assaf *et al.* (2011). These results showed broad agreement with the models of Gray *et al.* (2009). The maser peak lags the optical by stellar phase $\phi \sim 0.2$, the brightest masers occuring during ϕ $0.1 - 0.4$. We summarise here the preliminary polarization results.

2. Results

R Cas was observed in full polarization, to provide Stokes I, Q, U and V data cubes at spatial and spectral resolutions of approximately (40×20 μas^2, 0.2 km s^{-1}). Polarization calibration and measurements were made following the methods described by Kemball *et al.* (2009). The polarization detection threshold for individual components is $5\sigma_{\mathrm{rms}}$ and $m_\ell > 5\%$ or $m_c > 15\%$; lower thresholds are possible when averaging over larger spectral or spatial regions (including correction for Ricean bias).

2.1. *Linear Polarization*

Fig. 1 shows the orientation of the electric vector position angles, EVPA $= 0.5$ arctan(U/Q); the length of the vectors is proportional to the linearly polarized intensity $P = (Q^2 + U^2)^{1/2}$. The SiO maser emission is significantly linearly polarized. The percentage linear polarization (averaged over all features per epoch) is $m_{ell} \sim 11 \rightarrow 58\%$. m_{ell} exceeds 100% in some isolated features (Section 3.2).

We investigated the relationship between the EVPA and the radial direction with respect to the star, defined by the position angle in the plane of the sky, θ. Fig. 2 shows the proportion of the polarized emission within bins of (EVPA$-\theta$) in the whole SiO shell and in the inner shell (within the radius enclosing 25% of the total maser flux at each epoch). The thickness of the line is proportional to the logarithm of the total linearly polarized flux. For the first cycle ($\phi = 0.158$ to $\phi = 1.158$, 15 epochs), the polarized flux in the whole shell is dominated by emission with EVPA either parallel
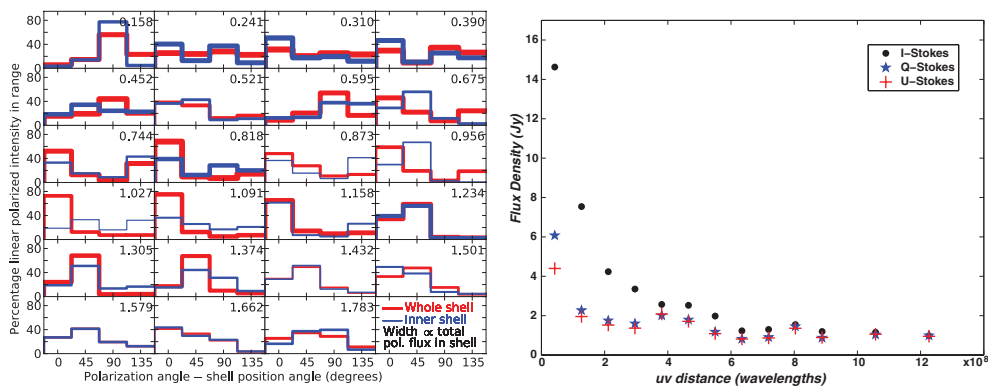
Figure 2. *Left* Histogram of the distribution of polarized emission with respect to the deviation of the polarization angle from the radial direction (EVPA$-\theta$). *Right* Stokes I, Q and U flux density as a function of baseline length for channels averaged from $24.8 - 29.4$ km s^{-1}, $\phi = 0.744$.

(10 epochs) or perpendicular (5 epochs) to θ. However, in the inner shell, only half the epochs have a high proportion of emission with parallel (6) or perpendicular (2) EVPA; it is at intermediate angles for the remaining 7 epochs. Seven out of the remaining 8 epochs (from $\phi = 1.234$ to $\phi = 1.783$), are dominated by emission with intermediate EVPA in the whole shell but this comes mainly from a single feature. At $\phi = 1.662$ the EVPA is predominantly parallel. The inner shell has more emission with a parallel EVPA at epochs $\phi = 1.501, 1.662$, otherwise behaving similarly to the whole shell.

The polarization structure during first stellar cycle can be summarised as a bimodal distribution. Most of the linear polarization vectors are either radial (parallel to the position angle of the location of the emission in the projected shell) or tangential (perpendicular). However, the polarization in the inner part of the shell is somewhat less ordered. The later parts of the second stellar cycle do not show any clear pattern, but the emission generally was noisier with fewer significantly polarized features.

2.2. Circular Polarization

Previous observations have shown that the mean degree of circular polarization in SiO masers is small but not zero, e.g. m$_c$ =1%-3% (Barvainis *et al.* 2009; Kemball& Diamond 1997). The average fractional circular polarization per epoch in R Cas is $m_c \sim 0.4 \to 6\%$. A few features showed 'S' shaped Stokes V profiles and we attempted to fit these with the function $V(\nu) = aI(\nu) + b(dI/d\nu)(\nu)$ ((Elitzur 1998)), but this did not succeed as V is very faint and the channel width is large compared with the Zeeman splitting.

3. Discussion

3.1. Linear polarization angle

In Section 2.1, we found that the linear polarization angle was predominantly parallel or perpendicular to the radial direction with respect to the star, in the plane of the sky. Fig. 3 shows a single maser feature (spanning ~ 2 km s^{-1}) with an abrupt transition in EVPA of approximately $\frac{\pi}{2}$. At this point, the linearly polarized intensity is near its minimum. The polarization vectors are tangential to the projected ring in the inner part of the feature and radial in its outer region. Goldreich *et al.* (1973) predicted this discontinuity in EVPA when the magnetic field direction with respect to the line of sight passes through θ_F , where $\sin^2 \theta_F = 2/3$. See Kemball *et al.* (2011) for a fuller description of this behaviour, observed in TX Cam.
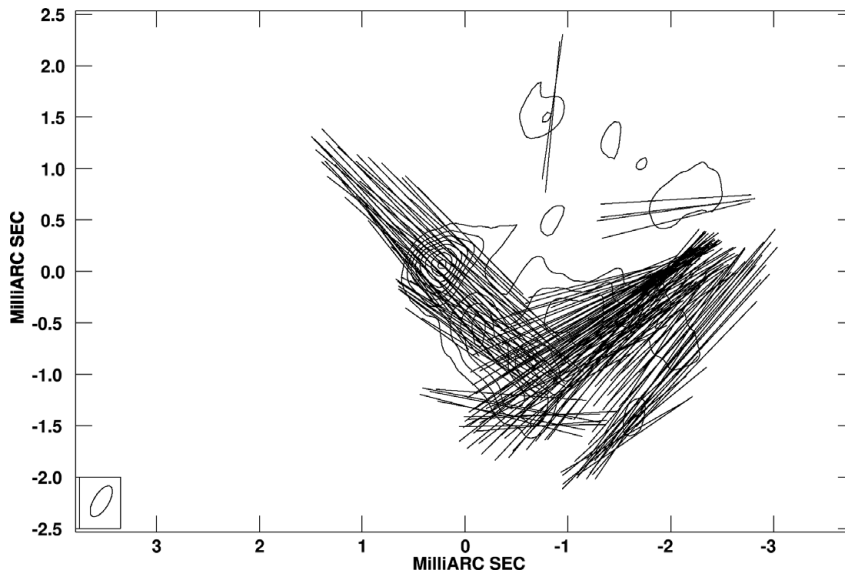
Figure 3. The blue-shifted maser feature seen in the NE, at around (20, 20) mas, averaged over V_{LSR} 25.6 – 27.43 km.s^{-1}, at $\phi = 0.818$ (Fig. 1). The vectors show the EVPA, length proportional to the polarized intensity.

3.2. *Fractional polarization*

We found that some isolated features are more than 100% linearly polarized. For instance, the clump at (25, 12) mas at $\phi = 0.744$ has 286% polarization. Fig. 2 (*right*) shows the visibility amplitudes for the channels including this clump (also containing others with smaller fraction polarization). The Stokes I flux density rises far more steeply on shorter baselines than does the polarized intensity. This suggests that a higher proportion of total intensity emission is on scales too large to be imaged on the shortest interferometer spacings, whilst a smaller proportion of polarized intensity is resolved-out. Polarization exceeding 100% has also been measured in the Galactic ISM (Haverkorn 2003a, b), explicable if the polarized emission has structure on smaller scales than the total intensity.

Kemball *et al.* (2009, 2011) explain why a magnetic origin is most likely for SiO polarization; the bulk kinetic energy density and the magnetic energy density are likely to be comparable, giving $B \sim 0.725$ G. Previously, it has been presumed that Faraday rotation ψ_F is negligible at the SiO wavelength $\lambda = 7$mm. We used the relation below from Garcia-Barreto *et al.* (1988):

$$\psi_F = 0.5 \left(\frac{n_e}{10^6 \, \text{cm}^{-3}} \right) \left(\frac{B_{||}}{\text{mG}} \right) \left(\frac{L}{10^{13} \, \text{m}} \right) \left(\frac{\lambda}{0.18 \text{m}} \right)^2 \qquad (3.1)$$

where $L \approx 2 \times 10^{11}$ m is the path length in the maser region (maser shell thickness). We estimated the electron density using the fractional ionisation model of Reid & Menten (1997) at number densities suitable for SiO masing, giving $n_e \sim 1.5 \times 10^9$ m^{-3}. The Faraday rotation is thus about 16°, small enough not to affect our inferences about the EPVA but sufficient to provide structure in the polarized emission.

4. Conclusions

The orientation of linear polarization vectors from the SiO masers around R Cas is consistent with a radial magnetic field. Where the masers come from material close

to the plane of the sky, the magnetic field is approximately perpendicular to the line of sight and the masers. Goldreich *et al.* (1973) predicts that the polarization angle would be perpendicular to the magnetic field direction. However, if the masing region has a significant depth, such that in some places the magnetic field is at $< 55°$ to the line of sight, the linear polarization angle would become parallel to the magnetic field. There is a systematic tendency for the maser polarization angle to be either parallel or perpendicular to the radial direction, and in some cases a local $90°$ change of direction in polarization angle seems to reflect the transition. The magnetic field is not more ordered in the inner shell, compared with the shell as a whole. This provides more evidence against anisotropic pumping as the main agent of maser polarization, since that would be most effective nearest the star.

The total intensity maser emission contains components which are smooth on scales larger than the maximum (< 1 AU) to which the VLBA is sensitive; the single dish flux density is several times greater than the correlated flux (Assaf *et al.* 2011). A few features with apparent linear polarization $\gg 100\%$ suggests that some factor affecting the propagation of polarized emission, e.g. the magnetic field, has structure on smaller scales. The magnetic field in the SiO maser region would produce Faraday rotation $\sim 15°$ (if the magnetic and bulk kinetic energy densities are similar) and local compression could enhance this.

References

Assaf, K. A., Diamond, P. J., Richards, A. M. S., & Gray, M. D. 2011, *MNRAS*, 415, 1083
Barvainis, Richard, McIntosh, Gordon, & Predmore, C. Read 1987, *Nature*, 329, 613.
Desmurs, J. F., Bujarrabal, V., Colomer, F., & Alcolea, J. 2000, *A&A*, 360, 189.
Elitzur, M. *ApJ*, 457, 415.
Elitzur, M. *ApJ*, 504, 390.
Garcia-Barreto, J. A., Burke, B. F., Reid, M. J., Moran, J. M., Haschick, A. D. & Schilizzi, R. T. 1988,*ApJ*, 326, 954.
Goldreich, P., Keeley, D. A., & Kwan, J. Y. 1973, *ApJ*, 179, 111.
Gonidakis, I., Diamond, P. J., & Kemball, A. J. 2010, *MNRAS*, 406, 395.
Gray M. D., Wittkowski, M., Scholz, M., Humphreys,E. M. L., Ohnaka K. & Boboltz, D. 2009,*MNRAS*, 394, 51.
Habing H. J. 1996,*A&AR*, 7, 97.
Haverkorn M. Katgert, P. & de Bruyn, A. G. 2003, *A&A*, 403, 1031.
Haverkorn M. Katgert, P. & de Bruyn, A. G. 2003, *A&A*, 404, 233.
Herpin, F., Baudry, A., Thum, C., Morris, D. & Wiesemeyer, H. 2006, *A&A*, 450, 667.
Kemball A. J. & Diamond P. J. 1997, *ApJ*, 481, L111.
Kemball, A. J., Diamond, P. J., Gonidakis, I., *et al.* 2009, *ApJ*, 698, 1721.
Kemball, A. J., Diamond, P. J., Richter, L., Gonidakis, I., & Xue, R. 2011, *ApJ*, 743, 69.
Reid, Mark J. & Menten, Karl M. 1997*ApJ*, 476, 327.
Troland, T. H., Heiles, C., Johnson, D. R., & Clark, F. O. 1979, *ApJ*, 232, 143.
Western, L. R. & Watson, W. D1983, *ApJ*, 275, 195.
Vlemmings, W. H. T., van Langevelde, H. J., Diamond, P. J., Habing, H. J., & Schilizzi, R. T. 2003, *A&A*, 407, 213.